



HAL
open science

Design and modeling of a passively Q-switched diode-pumped Thulium laser at $2.3 \mu\text{m}$

Esrom Kifle, Pavel Loiko, Lauren Guillemot, Jean-Louis Doualan, Florent Starecki, A. Braud, Ammar Hideur, Patrice Camy

► **To cite this version:**

Esrom Kifle, Pavel Loiko, Lauren Guillemot, Jean-Louis Doualan, Florent Starecki, et al.. Design and modeling of a passively Q-switched diode-pumped Thulium laser at $2.3 \mu\text{m}$. Optics Communications, 2021, 500, pp.127219. 10.1016/j.optcom.2021.127219 . hal-03345651

HAL Id: hal-03345651

<https://hal.science/hal-03345651>

Submitted on 7 Oct 2021

HAL is a multi-disciplinary open access archive for the deposit and dissemination of scientific research documents, whether they are published or not. The documents may come from teaching and research institutions in France or abroad, or from public or private research centers.

L'archive ouverte pluridisciplinaire **HAL**, est destinée au dépôt et à la diffusion de documents scientifiques de niveau recherche, publiés ou non, émanant des établissements d'enseignement et de recherche français ou étrangers, des laboratoires publics ou privés.

Design and modelling of a passively Q-switched diode-pumped Thulium laser at 2.3 μm

Esrom Kifle^a, Pavel Loiko^a, Lauren Guillemot^a, Jean-Louis Doualan^a, Florent Starecki^a, Alain Braud^a, Ammar Hideur^b, and Patrice Camy^{a,*}

^a*Centre de recherche sur les Ions, les Matériaux et la Photonique (CIMAP), UMR 6252 CEA-CNRS-ENSICAEN, Université de Caen, 6 Boulevard du Maréchal Juin, 14050 Caen Cedex 4, France*

^b*CORIA UMR6614, CNRS-INSA-Université de Rouen, Normandie Université, Avenue de l'université, BP. 12, 76801 Saint Etienne du Rouvray, France*

*Corresponding author, e-mail: patrice.camy@ensicaen.fr

Abstract. We report on a diode-pumped Tm:LiYF₄ laser operating on the $^3\text{H}_4 \rightarrow ^3\text{H}_5$ transition (at $\sim 2.3 \mu\text{m}$) passively Q-switched by a Cr²⁺:ZnSe saturable absorber. This laser delivers a maximum average output power of 130 mW at 2304.6 nm with a nearly diffraction limited beam, a linear polarization (π) and no colasing at $\sim 1.9 \mu\text{m}$. The corresponding pulse characteristics (duration / energy) are 1.24 μs / 3.6 μJ at a repetition rate of 36 kHz. By power scaling under quasi-CW pumping, even shorter pulse durations of 870 ns and higher pulse energies of 6.1 μJ are achieved. The performance of the laser is simulated using a model of a quasi-four-level gain medium and a “slow” saturable absorber showing a good agreement with the experiment. The effect of the thermal lens of the saturable absorber on the pulse characteristics is discussed.

Keywords: diode-pumped laser; thulium ions; passive Q-switching; mid-infrared; laser transition.

1. Introduction

Passive Q-switching is a well-known approach to generate pulsed output in solid-state lasers [1,2]. It is ensured by introducing into the laser cavity a nonlinear optical element, saturable absorber (SA). There are certain requirements for a SA: (i) it should provide linear absorption at the wavelength of laser emission, (ii) its transmission should decrease under high light intensity / fluence (absorption saturation or bleaching) recovering to the initial level after a relatively short time and (iii) it should possess high laser induced damage threshold (LIDT). Typically, SAs for passively Q-switched (PQS) near- and mid-IR solid-state lasers are made of crystals doped with transition metal (TM) ions such as Cr^{2+} , Fe^{2+} , Co^{2+} , V^{3+} , *etc.*, residing in tetrahedral (T_d) sites [3]. This is because tetrahedral coordination leads to high ground-state absorption (GSA) cross-sections for TM ions resulting in easy saturation of their linear absorption.

PQS lasers, as compared to their counterparts relying on active Q-switching, have the advantages of simple, compact and cost-effective design and the lack of external control elements.

Zinc chalcogenide crystals (ZnS and ZnSe) doped with chromium ions (Cr^{2+}) [4] are known as efficient SAs for lasers emitting at $\sim 2 \mu\text{m}$ [5], i.e., those based on thulium (Tm^{3+}) [6,7] and holmium (Ho^{3+}) [8,9] ions. This is because they provide broad and intense absorption bands owing to the $^5T_2 \rightarrow ^5E(^5D)$ transition of Cr^{2+} ions in T_d sites [10], high GSA cross-sections and weak excited-state absorption [11,12] and good thermal properties. In particular, Tm lasers emitting at $\sim 1.9 \mu\text{m}$ (the $^3F_4 \rightarrow ^3H_6$ transition) passively Q-switched by $\text{Cr}^{2+}:\text{ZnS}$ and $\text{Cr}^{2+}:\text{ZnSe}$ SAs and featuring both short pulse durations (down to sub-ns) [13] and relatively high pulse energies (mJ-level) [6,7,14] were demonstrated. Yu *et al.* reported on a Tm:LiLuF₄ laser PQS by $\text{Cr}^{2+}:\text{ZnS}$ and delivering 7.6 ns / 1.26 mJ (duration / energy) pulses at $\sim 1.9 \mu\text{m}$ [6]. Loiko *et al.* achieved sub-ns pulses (780 ps / 0.03 mJ) from a Tm:KLu(WO₄)₂ / $\text{Cr}^{2+}:\text{ZnS}$ microchip laser at $\sim 1.85 \mu\text{m}$ [13].

Besides the above mentioned $\sim 1.9 \mu\text{m}$ emission of Tm^{3+} ions, they can also provide laser action at $\sim 2.3 \mu\text{m}$ (the $^3H_4 \rightarrow ^3H_5$ transition) [15]. Such short-wavelength infrared (SWIR) emission is of practical importance for sensing of various atmospheric species (HF, CO, CH₄ and H₂CO) [16,17]. Although the $^3H_4 \rightarrow ^3H_5$ laser transition is known since many years [18], the interest to the development of continuous-wave (CW) [19-21] and pulsed (PQS [22,23] and mode-locked [24,25]) Tm lasers at $\sim 2.3 \mu\text{m}$ raised recently. Guillemot *et al.* reported on a CW Tm:KY₃F₁₀ laser delivering 0.84 W at 2331-2346 nm with a record-high slope efficiency of 53.8% (*vs.* the absorbed pump power) [26]. Canbaz *et al.* developed a Kerr-lens mode-locked Tm:LiYF₄ laser emitting 514 fs pulses at 2303 nm corresponding to a repetition rate of 41.5 MHz [25]. Note that in both studies, a high-brightness pump source (a Ti:Sapphire laser) was employed thus limiting the practical applications of such lasers.

However, so far, little attention was paid to PQS Tm lasers at $\sim 2.3 \mu\text{m}$ [22,23,27] and especially to the diode-pumped ones. Huang *et al.* developed a diode-pumped Tm:LiYF₄ laser PQS by $\text{Cr}^{2+}:\text{ZnSe}$ while the authors were not able get rid of the parasitic lasing at $\sim 1.9 \mu\text{m}$ [27]. The best pulse characteristics were 4 μs / 3.1 μJ and the average output power at 2306 nm – only 77 mW. Wang *et al.* studied a similar laser with a few-atomic-layer ReSe₂ SA and

reported on 0.71 μs / 97 μJ pulses [23]. However, the stability of the pulse train was low and secondary pulses were observed. Moreover, the practical applications of such SAs are very limited due to their low stability.

In the present work, we report on a diode-pumped Tm:LiYF₄ laser at ~ 2.3 μm PQS by Cr²⁺:ZnSe and delivering very stable pulsed output without any colasing at ~ 1.9 μm . The performance of the laser is modelled showing good agreement with the experiment.

2. Experimental

2.1. Laser set-up

The scheme of the laser set-up is shown in Fig. 1. For the laser experiments, we have selected a simple (linear) nearly hemispherical cavity to reduce the cavity roundtrip time and to shorten the Q-switched pulses. The cavity was formed by a flat pump mirror (PM) coated for high transmission (HT, $T = 94.4\%$) at 0.78 μm and for high reflection (HR) at 2.12 – 2.50 μm and two concave output couplers (OCs) with a radius of curvature (RoC) of -100 mm and a transmission T_{OC} of 0.7% and 1.3% ($\pm 0.2\%$) at 2.18 – 2.35 μm . The OCs provided HT ($T > 90\%$) at ~ 1.9 μm to suppress the oscillations at the competitive high-gain ${}^3\text{F}_4 \rightarrow {}^3\text{H}_6$ transition while no special coatings were provided for the PM.

As a gain material, we used tetragonal lithium yttrium fluoride crystal, Tm:LiYF₄. The laser element was cut for light propagation along the crystallographic *a*-axis (*a*-cut) giving access to both principal light polarizations (π and σ). The actual doping level determined by inductively coupled plasma mass spectrometry (ICP-MS) was 3.5 at.% Tm corresponding to the ion density N_{Tm} of 4.83×10^{20} cm^{-3} . The laser element had a cylindrical shape (diameter: $\Phi 8.5$ mm, thickness: $t = 8.1$ mm). Both faces were polished to laser-grade quality and antireflection (AR) coated at ~ 0.78 μm . The crystal was mounted on a massive Cu-holder from one of the faces leaving an opening in the centre using a silver paint for better heat removal. The holder was passively cooled. The crystal was placed close to the PM with a separation of ~ 5 mm. The geometrical length of the cavity was ~ 100 mm.

As a pump source, we used a CW fiber-coupled AlGaAs laser diode (DILAS, fiber core diameter: 105 μm , numerical aperture, N.A.: 0.22) emitting up to 20 W at ~ 788 nm (the ${}^3\text{H}_6 \rightarrow {}^3\text{H}_4$ transition of Tm³⁺ ions). The output from the laser diode was unpolarized and the measured emission bandwidth (FWHM) was ~ 3 nm. The estimated beam quality factor M^2 was ~ 45 (a nearly “top-hat” pump beam profile). The pump beam was collimated with an AR coated achromatic lens (focal length: $f = 50$ mm). The pump radiation was focused into the laser element through the PM using another AR-coated achromatic lens with $f = 60$ mm. The pump spot size (radius) in the focus was measured by the optical knife method to be $w_{\text{P}} = 78 \pm 10$ μm (at the $1/e^2$ level). To provide quasi-CW pumping, a mechanical chopper was inserted between the FL and CL (pulse duration: ~ 5 ms, duty cycle: 1:4).

The OCs provided high reflectivity at the pump wavelength. However, due to the strong pump divergence, the back-reflected pump was focused behind the crystal almost not contributing to the population inversion in the laser element. The absorbed pump power P_{abs} was calculated assuming single-pass pumping. The pump absorption under non-lasing (NL) conditions, $\eta_{\text{abs,NL}} = P_{\text{abs}}/P_{\text{inc}}$ (P_{inc} – the incident pump power) was estimated from the pump-

transmission experiment. Then, the pump absorption under lasing (L) conditions was determined from the $\eta_{\text{abs,NL}}$ value at the threshold pump power. It amounted to 53.3% ($T_{\text{OC}} = 0.7\%$) and 51.8% ($T_{\text{OC}} = 1.3\%$). The laser crystal was partially bleached.

A band-pass filter (FB2250-500, Thorlabs) was used to separate the laser emission from the residual (non-absorbed) pump. The spectra of laser emission were measured with an optical spectrum analyzer (OSA, AQ6375B, Yokogawa). The mode profile of the laser beam in the far-field was captured using a pyroelectric camera (PY-III-HR-C-A, Ophir) using a spherical uncoated CaF_2 lens ($f = 100$ mm) placed after the OC. The temporal behavior of the laser emission was studied using a fast InGaAs photodetector (model UPD-5N-IR2-P, rise time: <200 ps) and an 8 GHz digital oscilloscope (DSA70804B, Tektronix).

2.2. Saturable absorber

As a saturable absorber (SA) material, we have selected Cr^{2+} -doped chalcogenides (ZnS and ZnSe). In both materials, the chromium ions replaces for the Zn^{2+} ones in tetrahedral (T_d) sites giving rise to high ground-state absorption (GSA) cross-sections, σ_{GSA} , owing to the ${}^5T_2 \rightarrow {}^5E({}^5D)$ Cr^{2+} transition, weak excited-state absorption (ESA), low non-saturable losses and relatively fast recovery time τ_{rec} [4,11]. The σ_{GSA} spectra for Cr^{2+} -doped ZnS and ZnSe materials (measured in this work) are shown in Fig. 2(a). As one can see, the absorption band of chromium ions in ZnSe is red-shifted by about 75 nm as compared to its ZnS counterpart. Thus, $\text{Cr}^{2+}:\text{ZnSe}$ is more suitable for passive Q-switching of mid-IR lasers because of the higher GSA cross-sections. For $\text{Cr}^{2+}:\text{ZnSe}$ at the laser wavelength of 2.30 μm , σ_{GSA} is estimated from the measured GSA spectrum to be $0.024 \pm 0.01 \times 10^{-18}$ cm^2 . Although this value is much lower than the peak one, 0.98×10^{-18} cm^2 at 1.76 μm , it still provides a reasonable saturation fluence, $F_s = (h\nu_L)/\sigma_{\text{GSA}} = 3.6 \pm 1$ J/cm^2 , where h is the Planck constant and ν_L is the laser frequency. For $\text{Cr}^{2+}:\text{ZnSe}$, the ratio $\sigma_{\text{GSA}}/\sigma_{\text{ESA}}$ is <0.04 [11] and $\tau_{\text{rec}} = 5.4$ μs [28].

The SA fabricated from $\text{Cr}^{2+}:\text{ZnSe}$ had a cylindrical shape ($\Phi 12$ mm, $t = 1.0$ mm). Both its surfaces were polished with good parallelism and coated for HT ($T > 90\%$) at 2.0-2.3 μm . The calculated mean Cr^{2+} concentration was 2.2×10^{18} cm^{-3} . The small-signal (unsaturated) absorption due to the Cr^{2+} ions at the laser wavelength of 2.30 μm α'_{SA} was 0.5% (recalculated from the value specified at 1.76 μm). The optical losses originating from the polycrystalline ZnSe material α'_{loss} were about 1.8% (measured using a spectrophotometer), so that the small-signal transmission $T_{\text{SA}} = 1 - \alpha'_{\text{SA}} - \alpha'_{\text{loss}} \approx 97.6\%$.

To ensure passive Q-switching of the laser, the SA was inserted between the PM and the laser element at normal incidence. The air gap between the PM and the SA was ~ 1 mm. The SA was mounted on an Al-holder and passively cooled. The Cr^{2+} ions in T_d sites do not exhibit absorption at the pump wavelength of 0.78 μm , so that the SA heating by the pump was weak and provided mainly by the background absorption of the host material. This position of the SA almost in the waist of the laser mode (the calculated radius of the laser mode on the SA was 106 ± 6 μm) ensured its deep bleaching as compared to location between the crystal and the OC. The latter option may reduce the local heating of the SA, however, we

did not manage to achieve stable passive Q-switching in this geometry probably because of insufficient intracavity fluence.

3. Results and Discussion

3.1 Continuous-wave laser

To improve the thermal management of the laser (namely, to reduce the excessive heating of the passively cooled gain medium and the SA which may lead to serious Q-switching instabilities), the CW pumping was applied until an absorbed pump power P_{abs} of ~ 6.8 W. Above this power, the pumping was in quasi-CW regime.

Prior to the PQS experiment, we briefly characterized the laser performance without the SA in the cavity. The laser generated temporally stable output without instabilities or relaxation oscillations. Under CW pumping, the output power reached 0.63 W at 2302-2307 nm with a slope efficiency η of 14.3% (vs. the absorbed pump power) and a laser threshold of $P_{\text{th}} = 1.39$ W (for $T_{\text{OC}} = 1.3\%$), Fig. 3(a). A very similar performance was observed for $T_{\text{OC}} = 0.7\%$. The input-output dependences for both OCs were slightly nonlinear near the laser threshold and thus the fit yielding the slope efficiency was performed for pump powers well above P_{th} .

For quasi-CW pumping, the output dependences well matched those measured in the CW regime (for $P_{\text{abs}} < 6.8$ W) indicating weak thermal effects. Further increase of the pump power from the laser diode lead to a maximum average output power of 0.35 W (instantaneous peak power: 1.41 W) with higher $\eta = 20.8\%$, Fig. 3(b). The optical-to-optical efficiency η_{opt} (vs. the average incident pump power) reached 7.5% (all the values are specified for $T_{\text{OC}} = 1.3\%$). For $T_{\text{OC}} = 0.7\%$ under quasi-CW pumping, the laser performance was slightly inferior. These experiments confirm the possibilities for further power scaling if providing, e.g., active cooling of the laser element and SA.

The laser output was linearly polarized ($\mathbf{E} \parallel \mathbf{c}$, π -polarization) and the polarization state was naturally selected by the anisotropy of the gain. The spectra of laser emission were weakly dependent on T_{OC} being centred at ~ 2.30 μm , Fig. 4(a,b), well matching the main peak in the stimulated-emission (SE) cross-section, σ_{SE} , spectra for the ${}^3\text{H}_4 \rightarrow {}^3\text{H}_5$ transition of Tm^{3+} ions in LiYF_4 (the corresponding σ_{SE} value is 0.57×10^{-20} cm^2 at 2305 nm in π -polarization [19]). For CW operation (in the free-running regime, i.e., without any spectrally selective elements in the cavity), the spectra of laser emission were relatively broad spanning from 2302 to 2308 nm. This is ascribed to a relatively broad gain bandwidth of $\text{Tm}:\text{LiYF}_4$ (25.8 nm [19]).

3.2 Passively Q-switched laser: Power scaling

When inserting the SA into the laser cavity, very stable passively Q-switched operation was achieved. First, we studied the power transfer characteristics and the spectra of the PQS laser. We observed in this regime that the output coupling had a notable effect on the laser performance. Under CW pumping, for $T_{\text{OC}} = 1.3\%$, the maximum average output power reached 130 mW at 2304.6 nm with $\eta = 3.7\%$ and a laser threshold of 3.24 W, Fig. 3(a). For smaller $T_{\text{OC}} = 0.7\%$, the laser generated only 49 mW at 2304.7 nm with $\eta = 1.4\%$ and a

slightly lower threshold of 3.03 W. The increase of the laser threshold and the reduction in the slope efficiency as compared to the CW regime of operation is clearly related to the insertion loss of the SA (in particular, the background scattering loss of ZnSe and the losses at the dielectric coatings). Indeed, the Q-switching conversion efficiency with respect to the CW regime η_{conv} amounted to 20.6% ($T_{\text{OC}} = 1.3\%$) and 8.0% ($T_{\text{OC}} = 0.7\%$).

The possibility for further power scaling of the PQS laser was also demonstrated under quasi-CW pumping, Fig. 3(b). For the best-performing $T_{\text{OC}} = 1.3\%$, the average output power reached 89 mW with $\eta = 5.0\%$ and a Q-switching conversion efficiency $\eta_{\text{conv}} = 25.3\%$. It should be noticed that it was possible to operate the PQS laser under CW pumping at the expense of increased intensity instabilities in the Q-switched pulse train.

The typical spectra of the PQS laser are shown in Fig. 4. For both output couplers, the spectra were notably narrowed as compared to the CW regime which is related to competition of longitudinal modes bleaching the SA resulting in the filtering of some of them.

Both in the CW and PQS operation regimes, no colasing on the ${}^3F_4 \rightarrow {}^3H_6$ transition (at $\sim 1.9 \mu\text{m}$) was observed.

The PQS laser generated a nearly-circular beam and the 1D intensity profiles in the horizontal (x) and vertical (y , $\parallel c$ -axis) directions were well fitted with a Gaussian distribution (goodness of the fit: $R^2 > 0.99$). The measured beam quality factors $M^2_{x,y}$ were below 1.4. The spatial characteristics of the laser beam and their evaluation were similar to those described in the previous work [29].

3.3 Passively Q-switched laser: Pulse characteristics

Under CW pumping, the laser generated a continuous train of Q-switched pulses. The pulse duration (FWHM) $\Delta\tau$ and the pulse repetition frequency (PRF) were measured directly and the pulse energy was calculated, $E_{\text{out}} = P_{\text{out}}/\text{PRF}$, where P_{out} is the average output power. Under quasi-CW pumping, the laser generated regular bunches of pulses containing hundreds of pulses. The energy of an individual pulse was calculated as $E_{\text{out}} = 4P_{\text{out}}/\text{PRF}$ (for a duty cycle 1:4).

The pulse characteristics (duration and energy) of the PQS Tm:LiYF₄ laser are shown in Fig. 5. They exhibited a dependence on the pump power. For $T_{\text{OC}} = 1.3\%$ near the laser threshold, $\Delta\tau = 3.6 \mu\text{s}$, then it shortened with increasing the pump power and stabilized at $1.16 \pm 0.2 \mu\text{s}$. Nanosecond pulses ($\sim 870 \text{ ns}$) were achieved at intermediate power levels. For $T_{\text{OC}} = 0.7\%$, a similar behavior was observed while slightly longer pulse durations were obtained (stabilized at $1.30 \pm 0.15 \mu\text{s}$). Concerning the pulse energy, it slightly increased with the pump power and reached a maximum value of $6.1 \mu\text{J}$ and $3.5 \mu\text{J}$ for $T_{\text{OC}} = 1.3\%$ and 0.7% , respectively.

The pulse repetition frequency PRF of the PQS laser gradually increased with the pump power, Fig. 6, namely from 4.4 to 58.7 kHz (for $T_{\text{OC}} = 1.3\%$) and from 4.0 to 52.7 kHz (for $T_{\text{OC}} = 0.7\%$).

The typical oscilloscope traces of single Q-switched pulses from the PQS Tm:LiYF₄ laser are shown in Fig. 7. Here, we present the pulse corresponding to the maximum CW pump level ($P_{\text{abs}} = 6.7 \text{ W}$) and the shortest pulse observed at higher pump power of $P_{\text{abs}} \sim 8 \text{ W}$.

The pulses have a nearly Gaussian temporal shape. In Fig. 9(a,b), we present the typical oscilloscope traces of the pulse trains observed under CW pumping for the two studied output couplers. They confirm good stability of the PQS operation with intensity instabilities <7% and the r.m.s. pulse-to-pulse timing jitter of <5%. The PQS laser operated for tens of minutes without a noticeable deterioration of the output performance and Q-switching instabilities (for the range of pump powers applied for CW pumping). The Q-switching instabilities for the used laser design are mainly attributed to the heating of the SA by the pump radiation. In Fig. 9(c), we show a typical regular bunch of pulses under quasi-CW pumping.

3.4 Passively Q-switched laser: Simulation

$\text{Cr}^{2+}:\text{ZnSe}$ represents a “slow” saturable absorber for PQS mid-infrared lasers. This is because its recovery time of initial absorption ($\tau_{\text{rec}} = 5.4 \mu\text{s}$ [28]) that corresponds to the lifetime of the $^5\text{T}_2(^5\text{D}) \text{Cr}^{2+}$ state is longer than the characteristic time of formation of a single Q-switched pulse. For the designed laser with pulse durations of about $\sim 1 \mu\text{s}$, this condition is still satisfied. There exist a criterion for “slow” SA passive Q-switching [30]:

$$X = \frac{\sigma_{\text{GSA}}^{\text{L}} A_{\text{g}}}{\sigma_{\text{SE}}^{\text{L}} A_{\text{SA}}} \gg 1. \quad (1)$$

Here, $\sigma_{\text{GSA}}^{\text{L}}$ is the GSA cross-section of the SA and $\sigma_{\text{SE}}^{\text{L}}$ is the SE cross-section of the gain medium (both at the laser wavelength), and A_{g} and A_{SA} are the mode areas in the gain medium and the SA, respectively. Physically, the parameter X compares the saturation of the gain medium and the SA. If $X \gg 1$, the SA is deeply bleached and a weak dependence of pulse energy and duration on the pump power is observed, corresponding to generation of “giant” pulses. For the designed laser, $X = 6.1 > 1$ (this small value explains the variation of the pulse characteristics in Fig. 5).

The pulse energy and duration and the PRF were calculated using the model of a quasi-four-level gain medium (the $^3\text{H}_4 \rightarrow ^3\text{H}_5 \text{Tm}^{3+}$ transition) and a “slow” SA ($\text{Cr}^{2+}:\text{ZnSe}$) developed by Zhang *et al.* [2]. The main equations are given in Appendix A. The parameters of the cavity and the spectroscopic characteristics of the gain medium and the SA are listed in the text.

The results of the modelling are shown in Fig. 9 for the pulse duration and energy which are treated in the model as pump-independent values and in Fig. 6 (as curves) for the PRF which is pump-dependent. Let us first describe Fig. 9 where the parameters are calculated as a function of the output coupling ($T_{\text{OC}} = 0.1 - 7\%$) for several values of the saturable loss α'_{SA} ranging between 0.35% and 0.95%. The best agreement between the experiment and the model is observed for $\alpha'_{\text{SA}} = 0.55\%$ which agrees with the estimation from the transmission spectra (Section 2.2).

From Fig. 9(a), one can see that, for saturable losses $\alpha'_{\text{SA}} > 0.55\%$, the model predicts first a weak dependence of the pulse duration on the output coupling and then an abrupt rise of $\Delta\tau$. With increasing the saturable loss α'_{SA} , the range of T_{OC} values within which relatively short Q-switched pulses are expected becomes broader. As for the pulse energy, there exist an optimum output coupling leading to a maximum pulse energy at a given α'_{SA} . For higher saturable loss, this maximum shifts towards higher transmissions of the OC. For $T_{\text{OC}} = 1.3\%$,

the model predicts a pulse energy / duration of 4.8 μJ / 2.0 μs which reasonably agrees with the experiment. Moreover, Fig. 9(b) indicates that this output coupling is nearly optimum for the employed SA.

The pulse repetition frequency as a function of the pump power was also calculated for the two studied OCs, see the curves in Fig. 6. The model well describes the observed increase of the PRF with the pump power. For $T_{\text{OC}} = 1.3\%$ and $P_{\text{abs}} = 6.7 \text{ W}$ (the upper limit for CW pumping), it predicts a PRF of 33.8 kHz which agrees well with the experimental value (35.8 kHz).

During the PQS operation, no damage to the SA nor to the gain medium was observed. The intracavity axial peak fluence on the SA, calculated assuming a Gaussian spatial profile of the laser mode were $F_{\text{in}} = 4.73$ and 5.06 J/cm^2 for $T_{\text{OC}} = 1.3\%$ and 0.7% , respectively. These values are exceeding the calculated saturation fluence of the SA F_s , so that it is deeply bleached. Besides, the determined F_{in} values are below the LIDT for zinc chalcogenides (e.g., LIDT = $6.0 \pm 0.5 \text{ J/cm}^2$ for $\text{Cr}^{2+}:\text{ZnS}$ for ns pulses [12]).

3.5 Thermal lensing of the saturable absorber

The pump absorption in the SA ($\text{Cr}^{2+}:\text{ZnSe}$) may induce a thermal lens [31,32] which, in its turn, affects the size of the laser mode and the pulse characteristics of the PQS laser. For thin elements longitudinally pumped by a “top-hat” pump beam, the optical (refractive) power of the thermal lens $D = 1/f$ is expressed as [33]:

$$D_{\text{SA}} = \frac{\eta_{\text{abs}}^{\text{SA}} P_{\text{inc}}}{2\pi\kappa w_p^2} \chi_{\text{SA}}, \quad (2a)$$

$$\chi_{\text{SA}} = dn/dT + (n-1)(1+\nu)\alpha. \quad (2b)$$

Here, $\eta_{\text{abs}}^{\text{SA}} \approx 3.3\%$ is the absorption of the SA at the pump wavelength, Fig. 2(b), which is not saturated, P_{inc} is the incident pump power, $w_p \sim 450 \pm 100 \mu\text{m}$ is the pump spot radius on the SA (calculated using the ABCD formalism), $\kappa = 17.8 \text{ Wm}^{-1}\text{K}^{-1}$ is the thermal conductivity [34], $dn/dT = 5.34 \times 10^{-5} \text{ K}^{-1}$ is the thermo-optic coefficient, $n = 2.438$ is the refractive index at $2.30 \mu\text{m}$ [35,36], $\alpha = 7.8 \times 10^{-6} \text{ K}^{-1}$ [37] is the coefficient of thermal expansion and $\nu = 0.28$ is the Poisson ratio of the SA material (ZnSe). Equation 2(b) represents the term $\chi_{\text{SA}} = 6.74 \times 10^{-5} \text{ K}^{-1}$ which is called the “generalized” thermo-optic coefficient and it determines the sign of the thermal lens (positive). In Eq. (2b), we neglect the contribution of the photo-elastic effect which is relatively weak in cubic materials. Although the absorption in the SA is weak, the relatively large “generalized” thermo-optic coefficient of ZnSe may induce strong thermal lens.

For comparison, we also estimated the thermal lens of the diode-pumped laser crystal ($\text{Tm}:\text{LiYF}_4$) [33]:

$$D_{\text{AE}} = \frac{\eta_{\text{abs}} \eta_{\text{h,L}} P_{\text{inc}}}{2\pi \langle \kappa \rangle w_p^2} \chi_{\text{AE}}. \quad (3)$$

We used the same equation, only the factor of $\eta_{\text{abs}}^{\text{SA}}$ was replaced by $\eta_{\text{abs}} \eta_{\text{h,L}}$, and $\eta_{\text{abs}} = 51.8\%$ is the pump absorption under lasing conditions ($T_{\text{OC}} = 1.3\%$) and $\eta_{\text{h,L}} = 22.5\%$ is the fractional heat loading under lasing (L) conditions. The $\eta_{\text{h,L}}$ value was estimated from the

following considerations: the heat generation for a $\sim 2.3 \mu\text{m}$ laser originates mostly from the multi-phonon non-radiative relaxation from the lower laser level ($^3\text{H}_4$) to the metastable state ($^3\text{F}_4$). The latter manifold is mostly depopulated via radiative decay and this process does not generate heat. Thus, the fractional heat loading can be estimated as:

$$\eta_{h,L} \approx 1 - \frac{h\nu_L(2.3 \mu\text{m}) + h\langle\nu_{\text{lum}}\rangle(1.9 \mu\text{m})}{h\nu_P}, \quad (4)$$

where ν_L and ν_P are the laser and pump frequencies, respectively, and $\langle\nu_{\text{lum}}\rangle$ is the mean luminescence frequency (corresponding to $\langle\lambda_{\text{lum}}\rangle = 1824 \text{ nm}$ for Tm:LiYF₄). Finally, we achieve $\eta_h \approx 22.5\%$. This value reasonably agrees with the previously reported results for a Tm:YAG laser operating on the $^3\text{H}_4 \rightarrow ^3\text{H}_5$ transition, $\eta_h = 30\text{-}35\%$ well above the laser threshold [29]. The uncertainty in the estimation of the fractional heat loading is the main source of error in evaluating the thermal lens of the laser crystal. Other material parameters are as following: $\langle\kappa\rangle = 5.13 \text{ Wm}^{-1}\text{K}^{-1}$ [38] and $\chi_{\text{AE}} = -2.3 \times 10^{-6} \text{ K}^{-1}$ (specified for an *a*-cut crystal and π -polarization) [39].

The optical power of the thermal lens is pump-dependent, so that it is convenient to calculate the so-called sensitivity factor [40]:

$$M = \frac{dD}{dP_{\text{inc}}}. \quad (5)$$

For the SA (Cr²⁺:ZnSe) and the active element (Tm:LiYF₄), $M_{\text{SA}} = 0.096 \text{ m}^{-1}/\text{W}$ and $M_{\text{AE}} = -1.37 \text{ m}^{-1}/\text{W}$, respectively. Thus, the thermal lens in these two optical elements has different sign (it is positive in the SA and negative in the laser crystal). The thermal lens induced in the laser crystal is much stronger than that formed in the SA. Consequently, the thermal lens of the laser crystal is mainly responsible for the mode formation in the laser cavity.

Figure 10 presents the radii of the fundamental transverse mode in the center of the SA and the laser crystal as a function of the incident pump power calculated using the ABCD formalism and the determined *M*-factors of the thermal lenses. The mode radius in the laser crystal is weakly dependent on the pump power. However, the thermal lens of the laser crystal induces an increase of the mode radius on the SA, from $\sim 100 \mu\text{m}$ at the laser threshold of the PQS laser up to $\sim 112 \mu\text{m}$ at high pump powers. This will cause less deep bleaching of the SA and can partially explain the difference between the measured and calculated pulse characteristics.

As is it clear from Fig. 10, the thermal lens of the SA has a minor effect on the mode in the PQS laser cavity.

3.6 Discussion

In Table 1, we summarize the results on PQS Tm lasers operating on the $^3\text{H}_4 \rightarrow ^3\text{H}_5$ transition reported so far. In all the previous studies [22,23,27], Tm:LiYF₄ crystals were used as gain media and two types of SAs were employed, i.e., Cr²⁺:ZnSe (“slow” SA, the same as in the present work) and few-atomic layer ReSe₂ (“fast” SA).

The present work represents the first diode-pumped thulium laser operating solely at $\sim 2.3 \mu\text{m}$ (without colasing at $\sim 1.9 \mu\text{m}$) and generating very stable regular trains of pulses at relatively high repetition rates of tens of kHz. In terms of the average output power, we also

report on the best results as compared to the studies were Cr²⁺:ZnSe SAs were employed [22,27].

Canbaz *et al.* reported on a Tm:LiYF₄ / Cr²⁺:ZnSe laser [22], however, employing a diffraction-limited pump (a Ti:Sapphire laser) limiting its applications. Moreover, the average output power was low (27 mW at 2309 nm) and no information allowing to assess the pulse train stability was provided.

Huang *et al.* studied a similar laser with diode-pumping [27] which however exhibited simultaneous laser emission at 1.88 μm and 2.31 μm. This affected the stability of the PQS operation because pulse groups with a varying number of individual pulses (between few and 10 pulses) were observed.

Wang *et al.* employed few-atomic layer ReSe₂ SA in a diode-pumped Tm:LiYF₄ laser [23]. Few-atomic layer materials are of little practical use as they have limited stability under long-term operation. However, such SAs provide much lower insertion losses as compared to crystals doped with TM ions [9], so better power scaling capabilities are expected. In [23], the PQS laser generated irregular bunches of pulses; moreover, the presented oscilloscope traces indicated a possible CW component in the laser emission. Thus, the reported high pulse energy cannot be interpreted as a single-pulse energy.

4. Conclusion

To conclude, we report on the first diode-pumped passively Q-switched Thulium laser operating on the ³H₄ → ³H₅ transition (without colasing at ~1.9 μm) and generating very stable regular trains of ~1 μs-long single Q-switched pulses at high repetition rates of about few tens of kHz. This is due to (i) a combination of the gain material (Tm:LiYF₄) highly suitable for lasing at ~2.3 μm and the saturable absorber (Cr²⁺:ZnSe) ensuring reasonable saturation fluence at this laser wavelength; (ii) the use of spectrally-selective cavity mirrors suppressing the unwanted lasing at ~1.9 μm; (iii) a compact cavity design ensuring short cavity roundtrip time and deep bleaching of the SA. Passive Q-switching of ~2.3 μm Tm lasers is a complicated task due to the relatively short upper laser level (³H₄) lifetime (e.g., only 156 μs for 3.5 at.% Tm:LiYF₄ as used in the present work), low gain for the ³H₄ → ³H₅ transition and a strong competition with the high-gain ³F₄ → ³H₆ one.

Further improvement of the pulse characteristics of the Tm:LiYF₄ / Cr²⁺:ZnSe lasers seems to be possible by optimization of the cavity design. The use of an L-shaped cavity may simultaneously provide deep bleaching of the SA, eliminate its heating by the residual pump and ensure large mode area in the gain material leading to higher pulse energies. Going to a microchip-type design will result in generation of much shorter pulses of few tens of ns whilst at the expense of the low pulse energy. At a glance, better energy storage capabilities are expected with Tm:LiYF₄ crystals with lower doping leading to weaker self-quenching of the upper laser lifetime. However, as it was shown [19], higher doping levels enhance the performance of ~2.3 μm Tm lasers due to the energy-transfer upconversion. Thus, the search of an optimum doping level for PQS laser operation is needed.

Among the SAs based on transition-metal ions, Fe²⁺-doped ZnSe may be a good candidate for PQS of ~2.3 μm lasers due to its broadband absorption centered at ~3.1 μm and featuring high GSA cross-sections.

Declaration of competing interest

The authors declare that they have no known competing financial interests or personal relationships that could have appeared to influence the work reported in this paper.

Acknowledgements

This work was supported by French Agence Nationale de la Recherche (ANR) through the LabEx EMC3 (ANR-10-LABX-09-01), SPLENDID2 (ANR-19-CE08-0028), and the European project "NOVAMAT" co-funded by the Normandy County Council and the European Union within the framework of the Operational Program ERDF/ESF 2014-2020.

Appendix A

Expressions for calculating the pulse characteristics of a continuously-pumped PQS ~2.3 μm Thulium laser (after [2]). The pulse energy E_{out} and the peak power P_{peak} (the pulse duration: $\Delta\tau = E_{\text{out}}/P_{\text{peak}}$) are:

$$E_{\text{out}} = \frac{h\nu_L A_{\text{AE}}}{2\sigma_{\text{SE}}^L \gamma} \ln\left(\frac{1}{R_{\text{OC}}}\right) \ln\left(\frac{n_i}{n_f}\right), \quad (\text{A1})$$

$$P_{\text{peak}} = \frac{h\nu_L A_{\text{AE}} \ell}{2t_r} \cdot \ln\left(\frac{1}{R_{\text{OC}}}\right) \cdot \left[n_i - n_t - n_{t0} \ln\left(\frac{n_t}{n_i}\right) - (n_i - n_{t0}) \frac{1}{\alpha} \left(1 - \frac{n_t^\alpha}{n_i^\alpha}\right) \right]. \quad (\text{A2})$$

Here, h is the Planck constant, ν_L is the laser frequency, A_{AE} is the mode area in the active element and ℓ is its length, σ_{SE}^L is the SE cross-section at ν_L , γ is the inversion reduction factor, R_{OC} is the reflectivity of the OC, $t_r = 2\ell'/c$ is the cavity roundtrip time, ℓ' is the cavity optical length and c is the speed of light, $\alpha = \sigma_{\text{GSA}}/(\gamma\sigma_{\text{SE}}^L)$ is a factor concerning the saturation of the active element and the SA, and n_{t0} , n_i , n_t and n_f are determined from the following equations:

$$n_{t0} = \frac{-\ln(R_{\text{OC}}) - \delta \ln(T_{\text{SA}}^2) + L}{2\sigma_{\text{SE}}^L \ell}, \quad (\text{A3})$$

$$n_i = \frac{-\ln(R_{\text{OC}}) - \ln(T_{\text{SA}}^2) + L}{2\sigma_{\text{SE}}^L \ell}, \quad (\text{A4})$$

$$\frac{n_t}{n_i} = \frac{n_{t0}}{n_i} + \left(1 - \frac{n_{t0}}{n_i}\right) \left(\frac{n_t}{n_i}\right)^\alpha, \quad (\text{A5})$$

$$1 - \frac{n_f}{n_i} + \left(\frac{n_{t0}}{n_i}\right) \ln\left(\frac{n_f}{n_i}\right) - \left(1 - \frac{n_{t0}}{n_i}\right) \frac{1}{\alpha} \left(1 - \left(\frac{n_f}{n_i}\right)^\alpha\right) = 0. \quad (\text{A6})$$

Here, $\delta = \sigma_{\text{ESA}}/\sigma_{\text{GSA}}$ and σ_{ESA} is the ESA absorption cross-section of the SA, T_{SA} is the initial (small-signal) transmission of the SA at ν_L , and L is the roundtrip passive loss. Here, n is the instantaneous population inversion density: n_i – its initial value at the start of Q-switching, n_t

– its value at the moment of maximum power and n_f – its final value. The parameter n_{t0} has a meaning of n_t when $\alpha \rightarrow \infty$.

The pulse repetition frequency (PRF) is:

$$\text{PRF} = \frac{1}{\tau_{3\text{lum}}} \frac{(B/B_{\text{th}}) - (1 + \beta)/2}{1 - \beta}, \quad (\text{A7})$$

$$\beta = 1 - \frac{f_a}{\gamma} \left(1 - \frac{n_f}{n_i} \right), \quad (\text{A8})$$

where $\tau_{3\text{lum}}$ is the upper laser level ($^3\text{H}_4$) lifetime, B is the volumetric pump rate into the upper laser level, $B_{\text{th}} = n_i/\tau_{3\text{lum}}$ is the threshold pump rate, f_a is the Boltzmann occupation factor of the upper laser level. These equations correspond to the condition $B > 2B_{\text{th}}$ and describe high repetition rate lasers.

References

1. J.J. Degnan, Optimization of passively Q-switched lasers, *IEEE J. Quantum Electron.* 31 (1995) 1890-1901.
2. X. Zhang, S. Zhao, Q. Wang, Q. Zhang, L. Sun, S. Zhang, Optimization of Cr^{4+} -doped saturable-absorber Q-switched lasers, *IEEE J. Quantum Electron.* 33 (1997) 2286-2294.
3. A.M. Malyarevich, K.V. Yumashev, Saturable absorbers based on tetrahedrally coordinated transition-metal ions in crystals, *J. Appl. Spectr.* 76 (2009) 1-43.
4. S. B. Mirov, V. V. Fedorov, D. V. Martyshkin, I. S. Moskalev, M. S. Mirov, V. P. Gapontsev, Progress in mid-IR Cr^{2+} and Fe^{2+} doped II-VI materials and lasers, *Opt. Mater. Express* 1 (2011) 898-910.
5. T.-Y. Tsai, M. Birnbaum, Q-switched 2- μm lasers by use of a $\text{Cr}^{2+}:\text{ZnSe}$ saturable absorber, *Appl. Opt.* 40 (2001) 6633-6637.
6. H. Yu, V. Petrov, U. Griebner, D. Parisi, S. Veronesi, M. Tonelli, Compact passively Q-switched diode-pumped $\text{Tm}:\text{LiLuF}_4$ laser with 1.26 mJ output energy, *Opt. Lett.* 37 (2012) 2544-2546.
7. A. Korenfeld, D. Sebbag, U. Ben-Ami, E. Shalom, G. Marcus, S. Noach, High pulse energy passive Q-switching of a diode-pumped $\text{Tm}:\text{YLF}$ laser by $\text{Cr}:\text{ZnSe}$, *Laser Phys. Lett.* 12 (2015) 045804.
8. J. M. Serres, P. Loiko, X. Mateos, V. Jambunathan, A. S. Yasukevich, K. V. Yumashev, V. Petrov, U. Griebner, M. Aguiló, F. Díaz, Passive Q-switching of a $\text{Tm},\text{Ho}:\text{KLu}(\text{WO}_4)_2$ microchip laser by a $\text{Cr}:\text{ZnS}$ saturable absorber, *Appl. Opt.* 55 (2016) 3757-3763.
9. R. Lan, P. Loiko, X. Mateos, Y. Wang, J. Li, Y. Pan, S. Y. Choi, M. H. Kim, F. Rotermund, A. Yasukevich, K. Yumashev, U. Griebner, V. Petrov, Passive Q-switching of microchip lasers based on $\text{Ho}:\text{YAG}$ ceramics, *Appl. Opt.* 55 (2016) 4877-4887.
10. L. D. DeLoach, R. H. Page, G. D. Wilke, S. A. Payne, W. F. Krupke, Transition metal-doped zinc chalcogenides: spectroscopy and laser demonstration of a new class of gain media, *IEEE J. Quantum Electron.* 32 (1996) 885-895.
11. A. V. Podlipensky, V. G. Shcherbitsky, N. V. Kuleshov, V. P. Mikhailov, V. I. Levchenko, V. N. Yakimovich, $\text{Cr}^{2+}:\text{ZnSe}$ and $\text{Co}^{2+}:\text{ZnSe}$ saturable-absorber Q switches for 1.54- μm $\text{Er}:\text{glass}$ lasers, *Opt. Lett.* 24 (1999) 960-962.

12. P. Loiko, V. Vitkin, S. Balabanov, O. Dymshits, K. Grigorenko, A. Polishchuk, A. Volokitina, X. Mateos, J. M. Serres, E. Gavrishchuk, Saturable absorption properties at 1.54 μm of $\text{Cr}^{2+}:\text{ZnS}$ prepared by thermal diffusion at hot isostatic pressing, *Laser Phys. Lett.* 16 (2019) 065801-1-6.
13. P. Loiko, J.M. Serres, X. Mateos, K. Yumashev, A. Yasukevich, V. Petrov, U. Griebner, M. Aguiló, F. Díaz, Subnanosecond $\text{Tm}:\text{KLuW}$ microchip laser Q-switched by a $\text{Cr}:\text{ZnS}$ saturable absorber, *Opt. Lett.* 40 (2015) 5220-5223.
14. R. Faoro, M. Kadankov, D. Parisi, S. Veronesi, M. Tonelli, V. Petrov, U. Griebner, M. Segura, X. Mateos, Passively Q-switched $\text{Tm}:\text{YLF}$ laser,"*Opt. Lett.* 37 (2012) 1517-1519.
15. J.F. Pinto, L. Esterowitz, G.H. Rosenblatt, $\text{Tm}^{3+}:\text{YLF}$ laser continuously tunable between 2.20 and 2.46 μm , *Opt. Lett.* 19 (1994) 883–885.
16. A. Garnache, A. Liu, L. Cerutti, A. Campargue, Intracavity laser absorption spectroscopy with a vertical external cavity surface emitting laser at 2.3 μm : Application to water and carbon dioxide, *Chem. Phys. Lett.* 416 (2005) 22-27.
17. F.J. McAleavey, J. O’Gorman, J.F. Donegan, B. D. MacCraith, J. Hegarty, G. Mazé, Narrow linewidth, tunable Tm^{3+} -doped fluoride fiber laser for optical-based hydrocarbon gas sensing, *IEEE J. Sel. Top. Quantum Electron.* 3 (1997) 1103–1111.
18. J. Caird, L. DeShazer, J. Nella, Characteristics of room-temperature 2.3- μm laser emission from Tm^{3+} in YAG and YAlO_3 , *IEEE J. Quantum Electron.* 11 (1975) 874-881.
19. P. Loiko, R. Soulard, L. Guillemot, G. Brasse, J.-L. Doualan, A. Braud, A. Tyazhev, A. Hideur, B. Guichardaz, F. Druon, P. Camy, Efficient $\text{Tm}:\text{LiYF}_4$ lasers at ~ 2.3 μm : Effect of energy-transfer upconversion, *IEEE J. Quantum Electron.* 55 (2019) 1700212.
20. A. Muti, M. Tonelli, V. Petrov, A. Sennaroglu, Continuous-wave mid-infrared laser operation of $\text{Tm}^{3+}:\text{KY}_3\text{F}_{10}$ at 2.3 μm , *Opt. Lett.* 44 (2019) 3242–3245.
21. L. Guillemot, P. Loiko, E. Kifle, J.-L. Doualan, A. Braud, F. Starecki, T. Georges, J. Rouvillain, A. Hideur, P. Camy, Watt-level mid-infrared continuous-wave $\text{Tm}:\text{YAG}$ laser operating on the ${}^3\text{H}_4 \rightarrow {}^3\text{H}_5$ transition, *Opt. Mater.* 101 (2020) 109745-1-8.
22. F. Canbaz, I. Yorulmaz, A. Sennaroglu, 2.3- μm $\text{Tm}^{3+}:\text{YLF}$ laser passively Q-switched with a $\text{Cr}^{2+}:\text{ZnSe}$ saturable absorber, *Opt. Lett.* 42 (2017) 1656-1659.
23. S. Wang, H. Huang, H. Chen, X. Liu, S. Liu, J. Xu, D. Shen, High efficiency nanosecond passively Q-switched 2.3 μm $\text{Tm}:\text{YLF}$ laser using a ReSe_2 -based saturable output coupler," *OSA Continuum* 2 (2019) 1676-1682.
24. R. Soulard, A. Tyazhev, J.-L. Doualan, A. Braud, A. Hideur, M. Laroche, B. Xu, P. Camy, 2.3 μm $\text{Tm}^{3+}:\text{YLF}$ mode-locked laser, *Opt. Lett.* 42 (2017) 3534–3536.
25. F. Canbaz, I. Yorulmaz, and A. Sennaroglu, Kerr-lens mode-locked 2.3- μm $\text{Tm}^{3+}:\text{YLF}$ laser as a source of femtosecond pulses in the mid-infrared, *Opt. Lett.* 42 (2017) 3964-3967.
26. L. Guillemot, P. Loiko, R. Soulard, A. Braud, J.-L. Doualan, A. Hideur, P. Camy, Close look on cubic $\text{Tm}:\text{KY}_3\text{F}_{10}$ crystal for highly efficient lasing on the ${}^3\text{H}_4 \rightarrow {}^3\text{H}_5$ transition," *Opt. Express* 28 (2020) 3451-3463.
27. H. Huang, S. Wang, H. Chen, O. L. Antipov, S. S. Balabanov, D. Shen, High power simultaneous dual-wavelength CW and passively-Q-switched laser operation of LD pumped $\text{Tm}:\text{YLF}$ at 1.9 and 2.3 μm , *Opt. Express* 27 (2019) 38593-38601.
28. S. Mirov, V. Fedorov, I. Moskalev, D. Martyshkin, C. Kim, Progress in Cr^{2+} and Fe^{2+} doped mid-IR laser materials, *Laser Photon. Rev.* 4 (2010) 21-41.

29. E. Kifle, P. Loiko, L. Guillemot, J.-L. Doualan, F. Starecki, A. Braud, T. Georges, J. Rouvillain, and P. Camy, Watt-level diode-pumped thulium lasers around 2.3 μm , *Appl. Opt.* 59 (2020) 7530-7539.
30. A. E. Siegman, *Lasers*. Univ. Sci. Books, Mill Valley, CA, 1986, pp. 1024–1028.
31. J. Song, C. Li, K.I. Ueda, Thermal influence of saturable absorber in passively Q-switched diode-pumped cw Nd:YAG/Cr⁴⁺:YAG laser, *Opt. Commun.* 177 (2000) 307-316.
32. A. Sennaroglu, Continuous-wave power transmission and thermal lensing of a saturable absorber subject to excited-state absorption, *Appl. Opt.* 38 (1999) 3334-3337.
33. S. Chénais, F. Druon, S. Forget, F. Balembois, P. Georges, On thermal effects in solid-state lasers: The case of ytterbium-doped materials, *Progr. Quantum Electron.* 30 (2006) 89-153.
34. N. Sankar, K. Ramachandran, On the thermal and optical properties of ZnSe and doped ZnSe crystals grown by PVT, *J. Cryst. Growth* 247 (2003) 157-165.
35. D.T.F. Marple, Refractive index of ZnSe, ZnTe, and CdTe, .
36. R.J. Harris, G.T. Johnston, G.A. Kepple, P.C. Krok, H. Mukai, Infrared thermo-optic coefficient measurement of polycrystalline ZnSe, ZnS, CdTe, CaF₂, and BaF₂, single crystal KCl, and TI-20 glass, *Appl. Opt.* 16 (1977) 436-438.
37. J.S. Browder, S.S. Ballard, Thermal expansion data for eight optical materials from 60 K to 300 K, *Appl. Opt.* 16 (1977) 3214-3217.
38. R.L. Aggarwal, D.J. Ripin, J.R. Ochoa, T.Y. Fan, Measurement of thermo-optic properties of Y₃Al₅O₁₂, Lu₃Al₅O₁₂, YAlO₃, LiYF₄, LiLuF₄, BaY₂F₈, KGd(WO₄)₂, and KY(WO₄)₂ laser crystals in the 80–300 K temperature range, *J. Appl. Phys.* 98 (2005) 103514.
39. Value provided by Prof. K. V. Yumashev (private communication).
40. P. Loiko, S. Manjooran, K. Yumashev, A. Major, Polarization anisotropy of thermal lens in Yb:KY(WO₄)₂ laser crystal under high-power diode pumping, *Appl. Opt.* 56 (2017) 2937-2945.

List of figure captions

Figure 1. Scheme of the diode-pumped Tm:LiYF₄ laser Q-switched by the Cr²⁺:ZnSe SA: LD – laser diode, CL and FL – collimating and focusing lens, respectively, PM – pump mirror, SA – saturable absorber, OC – output coupler, F – cut-off filter.

Figure 2. Saturable absorber: (a) Ground-state absorption cross-sections, σ_{GSA} , for Cr²⁺ ions in ZnS and ZnSe materials; (b) Small-signal intrinsic transmission (T_{SA}) spectrum (subtracting the effect from the coatings) of the Cr²⁺:ZnSe SA ($t = 1.0$ mm). The *arrows* in (a,b) indicate the pump (0.79 μm) and laser (2.30 μm) wavelengths.

Figure 3. Input-output dependences for the CW and Cr²⁺:ZnSe PQS diode-pumped Tm:LiYF₄ lasers: (a) CW pumping, (b) quasi-CW pumping (duty cycle: 1:4), η – slope efficiency.

Figure 4. Typical spectra of laser emission for the CW and Cr²⁺:ZnSe PQS diode-pumped Tm:LiYF₄ lasers: (a) $T_{\text{OC}} = 0.7\%$, (b) $T_{\text{OC}} = 1.3\%$. $P_{\text{abs}} \sim 6$ W. The laser polarization is π .

Figure 5. Pulse characteristics: (a) duration (FWHM) and (b) energy for the diode-pumped Tm:LiYF₄ laser PQS by a Cr²⁺:ZnSe SA.

Figure 6. Pulse repetition frequency for the diode-pumped Tm:LiYF₄ laser PQS by a Cr²⁺:ZnSe SA: *symbols* – experimental data, *curves* – modelling.

Figure 7. Oscilloscope traces of single Q-switched pulses from the diode-pumped Tm:LiYF₄ laser PQS by a Cr²⁺:ZnSe SA (the pulses observed at the maximum CW pump power of $P_{\text{abs}} = 6.7$ W and the shortest pulses are shown): (a) $T_{\text{OC}} = 1.3\%$, (b) $T_{\text{OC}} = 0.7\%$.

Figure 8. Oscilloscope traces of pulse trains from the diode-pumped Tm:LiYF₄ laser PQS by a Cr²⁺:ZnSe SA: (a,b) CW pumping, (a) $T_{\text{OC}} = 1.3\%$, $P_{\text{abs}} = 5.45$ W, (b) $T_{\text{OC}} = 0.7\%$, $P_{\text{abs}} = 6.23$ W; (c) quasi-CW pumping, $T_{\text{OC}} = 1.3\%$, $P_{\text{abs}} = 8.27$ W.

Figure 9. Simulation of (a) the pulse duration and (b) the pulse energy for the diode-pumped Tm:LiYF₄ laser PQS by a Cr²⁺:ZnSe SA: curves – calculated dependences of the pulse characteristics on the transmission of the output coupler T_{OC} for various values of the saturable loss α'_{SA} , symbols – experimental data.

Figure 10. Simulation of the radius of the fundamental transverse mode in the center of the SA (Cr²⁺:ZnSe) and laser crystal (Tm:LiYF₄) in the diode-pumped PQS laser: *solid curves* – accounting for the thermal lenses in both elements, *dashed curves* – accounting only for the thermal lens of the laser crystal. *Vertical line*: laser threshold for $T_{OC} = 1.3\%$.

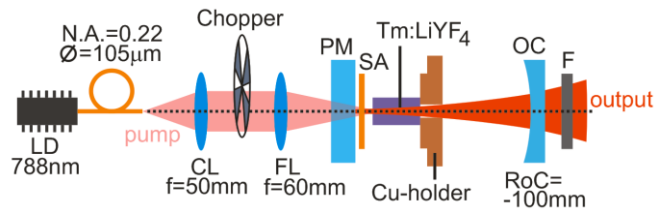


Figure 1. Scheme of the diode-pumped Tm:LiYF₄ laser Q-switched by the Cr²⁺:ZnSe SA: LD – laser diode, CL and FL – collimating and focusing lens, respectively, PM – pump mirror, SA – saturable absorber, OC – output coupler, F – cut-off filter.

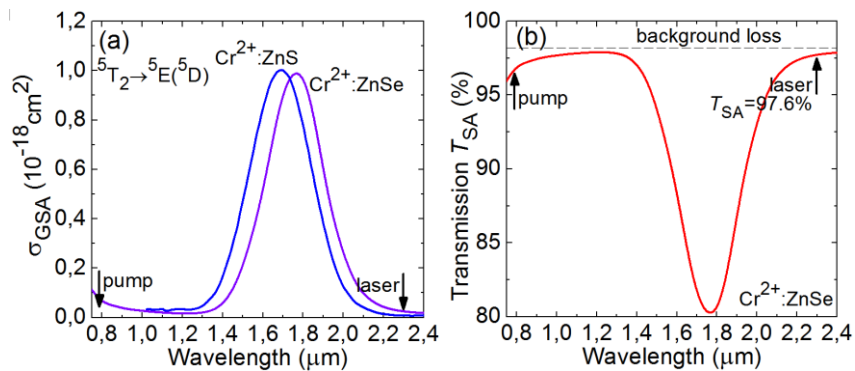


Figure 2. Saturable absorber: (a) Ground-state absorption cross-sections, σ_{GSA} , for Cr²⁺ ions in ZnS and ZnSe materials; (b) Small-signal intrinsic transmission (T_{SA}) spectrum (subtracting the effect from the coatings) of the Cr²⁺:ZnSe SA ($t = 1.0$ mm). The arrows in (a,b) indicate the pump (0.79 μm) and laser (2.30 μm) wavelengths.

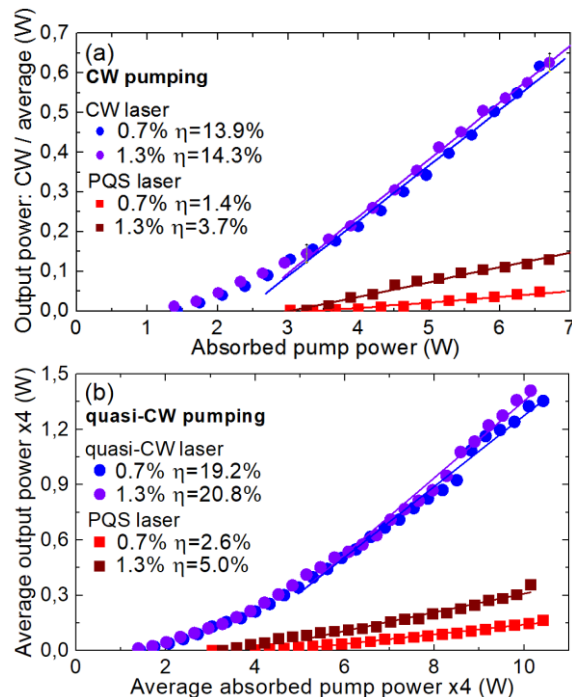


Figure 3. Input-output dependences for the CW and Cr²⁺:ZnSe PQS diode-pumped Tm:LiYF₄ lasers: (a) CW pumping, (b) quasi-CW pumping (duty cycle: 1:4), η – slope efficiency.

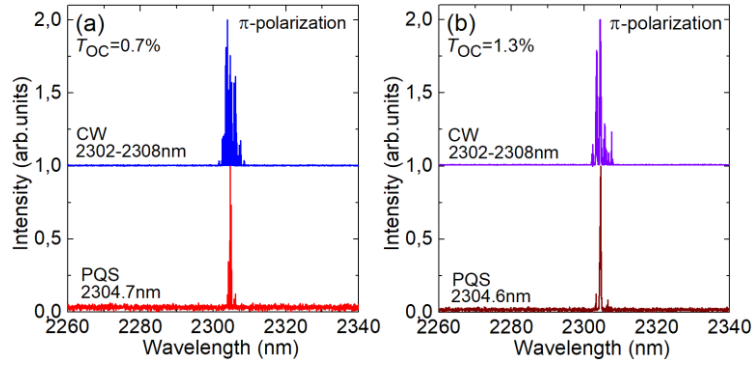


Figure 4. Typical spectra of laser emission for the CW and $\text{Cr}^{2+}:\text{ZnSe}$ PQS diode-pumped $\text{Tm}:\text{LiYF}_4$ lasers: (a) $T_{\text{OC}} = 0.7\%$, (b) $T_{\text{OC}} = 1.3\%$. $P_{\text{abs}} \sim 6 \text{ W}$. The laser polarization is π .

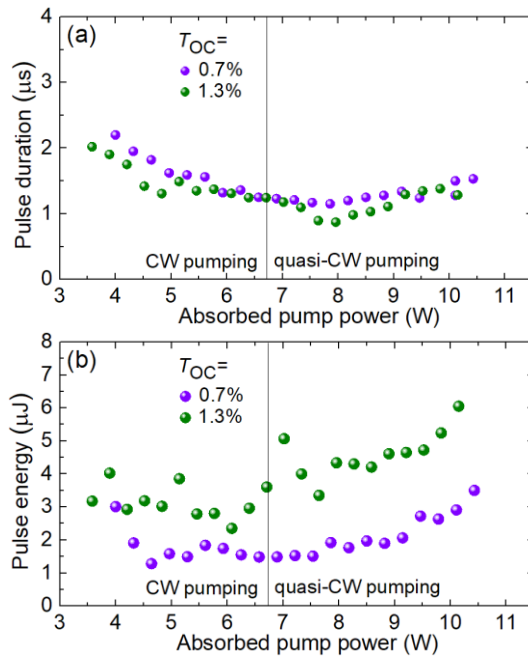


Figure 5. Pulse characteristics: (a) duration (FWHM) and (b) energy for the diode-pumped $\text{Tm}:\text{LiYF}_4$ laser PQS by a $\text{Cr}^{2+}:\text{ZnSe}$ SA.

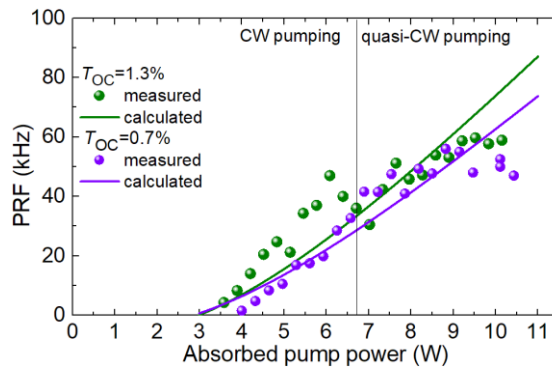


Figure 6. Pulse repetition frequency for the diode-pumped $\text{Tm}:\text{LiYF}_4$ laser PQS by a $\text{Cr}^{2+}:\text{ZnSe}$ SA: *symbols* – experimental data, *curves* – modelling.

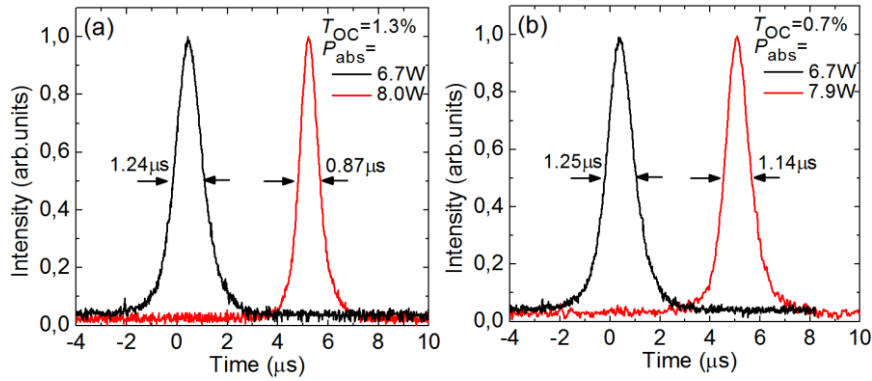


Figure 7. Oscilloscope traces of single Q-switched pulses from the diode-pumped Tm:LiYF₄ laser PQS by a Cr²⁺:ZnSe SA (the pulses observed at the maximum CW pump power of $P_{\text{abs}} = 6.7$ W and the shortest pulses are shown): (a) $T_{\text{OC}} = 1.3\%$, (b) $T_{\text{OC}} = 0.7\%$.

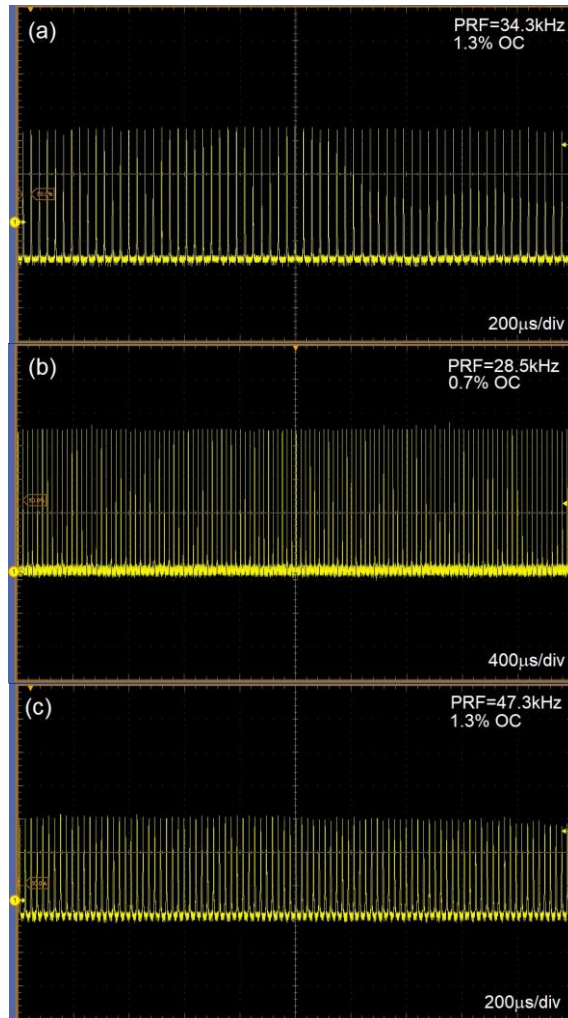


Figure 8. Oscilloscope traces of pulse trains from the diode-pumped Tm:LiYF₄ laser PQS by a Cr²⁺:ZnSe SA: (a,b) CW pumping, (a) $T_{\text{OC}} = 1.3\%$, $P_{\text{abs}} = 5.45$ W, (b) $T_{\text{OC}} = 0.7\%$, $P_{\text{abs}} = 6.23$ W; (c) quasi-CW pumping, $T_{\text{OC}} = 1.3\%$, $P_{\text{abs}} = 8.27$ W.

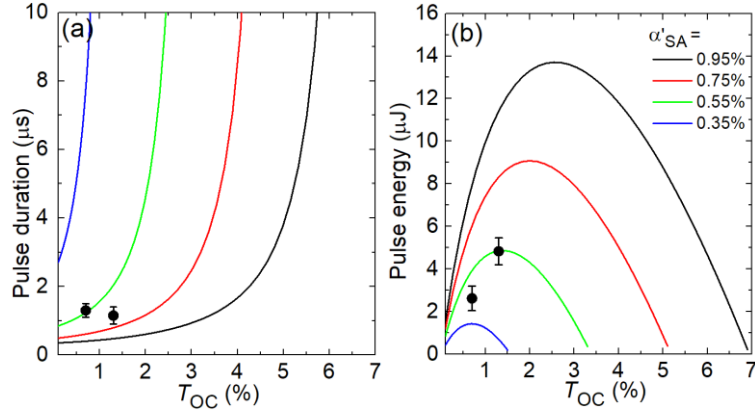


Figure 9. Simulation of (a) the pulse duration and (b) the pulse energy for the diode-pumped Tm:LiYF₄ laser PQS by a Cr²⁺:ZnSe SA: curves – calculated dependences of the pulse characteristics on the transmission of the output coupler T_{OC} for various values of the saturable loss α'_{SA} , symbols – experimental data.

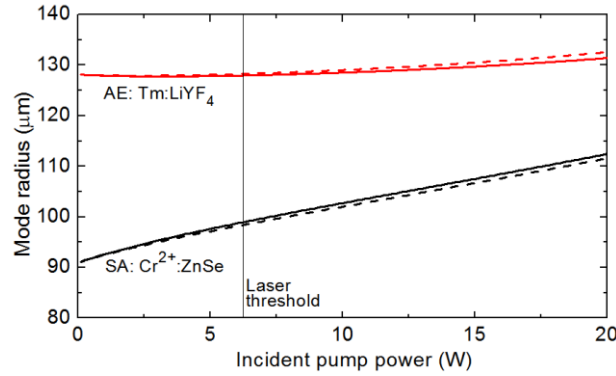


Figure 10. Simulation of the radius of the fundamental transverse mode in the center of the SA (Cr²⁺:ZnSe) and laser crystal (Tm:LiYF₄) in the diode-pumped PQS laser: *solid curves* – accounting for the thermal lenses in both elements, *dashed curves* – accounting only for the thermal lens of the laser crystal. *Vertical line*: laser threshold for $T_{OC} = 1.3\%$.

Table 1. Output characteristics^a of passively Q-switched $\sim 2.3 \mu\text{m}$ Tm:LiYF₄ lasers reported so far.

Pump ^b	SA	P_{out} , mW	λ_L , nm	η , %	η_{conv} , %	$\Delta\tau$, μs	E_{out} , μJ	PRF, kHz	Ref.
TS	Cr ²⁺ :ZnSe	27	2309	~ 4	~ 18	1.3	13	2.1	[22]
LD	Cr ²⁺ :ZnSe	77 + 202	2306 + 1880	~ 6	6.9	4	3.1	24.8	[27]
LD	ReSe ₂	486	2306	9	42.3	0.72	97.2 ^c	5.0	[23]
LD	Cr ²⁺ :ZnSe	130 89 ^d	2304.6 2304.6	3.7 5.0	20.6 25.3	1.24 1.30	3.6 6.1	36.1 59.2	This work

^a P_{out} – average output power, λ_L – laser wavelength, η – slope efficiency, η_{conv} – Q-switching conversion efficiency, $\Delta\tau$ – pulse duration, E_{out} – pulse energy, PRF – pulse repetition frequency.

^bTS – Ti:Sapphire laser, LD – laser diode.

^cTotal energy for a bunch of pulses.

^dQuasi-CW pumping with a duty cycle of 1:4.